Inhibition of G_1 to S Phase Progression by a Novel Zinc Finger Protein $P58^{TFL}$ at P-bodies

Kentaro Minagawa, Yoshio Katayama, Shinichiro Nishikawa, Katsuya Yamamoto, Akiko Sada, Atsuo Okamura, Manabu Shimoyama, and Toshimitsu Matsui

Hematology/Oncology, Department of Medicine, Kobe University Graduate School of Medicine, Kobe, Japan

Abstract

We recently reported the translocation of the *immunoglobulin (Ig) light chain κ locus gene* with a possible tumor suppressor gene, *TFL*, in transformed follicular lymphoma. However, the functional significance in cell transformation remains to be elucidated. Here, we first identified two gene products, $P58^{TFL}$ and $P36^{TFL}$, derived by alternative splicing. The expression was prominent in normal human lymphocytes but defective in some leukemia/lymphoma cell lines. Overexpression of either protein in a mouse pro-B cell line, Ba/F3, and a human leukemia cell line, Jurkat, inhibited G_1 to S phase progression through suppression of retinoblastoma protein (Rb) phosphorylation. The dominant gene product, $P58^{TFL}$, colocalized with mRNA-processing body markers, eukaryotic translation initiation factor 2C and DCP1 decapping-enzyme homolog A, but not with a stress granule maker, T-cell intracellular antigen 1, in the cytoplasm. Taken together with the unique CCCH-type zinc finger motif, the present study suggests that $P58^{TFL}$ could play an important role in the regulation of cell growth through posttranscriptional modification of cell cycle regulators, at least partially, upstream of Rb. (Mol Cancer Res 2009;7(6):880–9)

Introduction

Cytogenetic abnormalities contribute not only to cancer initiation but also to tumor progression for many types of malignancies derived from hematopoietic, mesenchymal, and epithelial tissues (1-5). Neither the *BCR/ABL* fusion protein derived from Philadelphia chromosomes in chronic myeloid leukemia (6, 7) nor BCL-2 overexpression due to the *BCL-2* translocation to the *immunoglobulin loci* in B-cell lymphomas is capable of triggering cell transformation by itself (8, 9). Another genetic mutation is required for full transformation. For example, additional cytogenetic mutations are well documented in chronic myelogenous leukemia blast crisis. Similarly, in the transformation of *BCL-2*–positive follicular lymphoma into aggressive lymphoma, many cytogenetic abnormalities have been reported (10). Among them, loss of regions in the long arm of chromosome 6 (6q), which is frequently observed not only in hematologic but also in epithelial malignancies (11, 12), has been reported to be associated with poor prognosis (13, 14). These findings suggest the existence of an as yet uncharacterized tumor suppressor gene on 6q21-25.

To pave the way for identification of tumor suppressor gene candidates, microarrays such as array based-comparative genomic hybridization, which can visualize gene amplification and/or other defects in cancer, have been used by several groups around the world. Indeed, loss of 6q21-q27 was reported to be frequent in B-cell lymphoma (15, 16).

Alternatively, a rare cytogenetic translocation sometimes reveals a novel oncogene or cryptic mutation important for tumorigenesis or leukemogenesis. For example, the tumor suppressor gene *HACE1* was first identified from a t(6;15) translocation in a Wilms' tumor sample. Thereafter, *HACE1* was shown to be involved in multiple cancers (17, 18). The universal cryptic defect of the α-type platelet-derived growth factor receptor gene (*αPDGFR*) in chronic eosinophilic leukemia was also first identified from a rare case with t(1;4)(q44;q12) (ref. 19). Thereafter, the genetic change established a new clinical entity defined in the updated WHO classification (20).

Recently, we identified a possible tumor suppressor gene at the break points of the t(2;6)(p12;q25) translocation in a transformed follicular lymphoma, designated *TFL* (21, 22). The break point was located at the putative second intron of *ZC3H12D*, an orphan gene previously defined by the human genome project (GenBank accession no. NM 207360). The gene presumably encodes a single "Cys-x8-Cys-x5-Cys-x3-His" (CCCH)-type zinc finger protein, and was recently reported to be a novel tumor suppressor gene candidate. Its loss of heterozygosity was found in sporadic lung cancer, and a single-nucleotide polymorphism at codon 106 was shown to affect tumor growth (23).

However, the *TFL* gene structure, its gene products, or their physiologic function has not yet been determined. Reports of the exon organization of *ZC3H12D* transcripts have been frequently rewritten on the web site of National Center for Biotechnology Information (NCBI). To clarify the functional significance of this tumor suppressor gene candidate in cell transformation, we investigated the *TFL* gene products and their expression profiles and biological function.

Received 10/31/08; revised 1/7/09; accepted 2/12/09; published OnlineFirst 6/16/09.
Grant support: Grants-in-aid for scientific research from the Ministry of Education, Culture, Sports, Science and Technology of Japan.
The costs of publication of this article were defrayed in part by the payment of page charges. This article must therefore be hereby marked *advertisement* in accordance with 18 U.S.C. Section 1734 solely to indicate this fact.
Note: Supplementary data for this article are available at Molecular Cancer Research Online (http://mcr.aacrjournals.org/).
Requests for reprints: Toshimitsu Matsui, Hematology/Oncology, Department of Medicine, Kobe University Graduate School of Medicine, 7-5-1, Kusunoki-cho, Chuo-ku, Kobe 650-0017, Japan. Phone: 81-78-382-5885; Fax: 81-78-382-5899. E-mail: matsui@med.kobe-u.ac.jp

doi:10.1158/1541-7786.MCR-08-0511

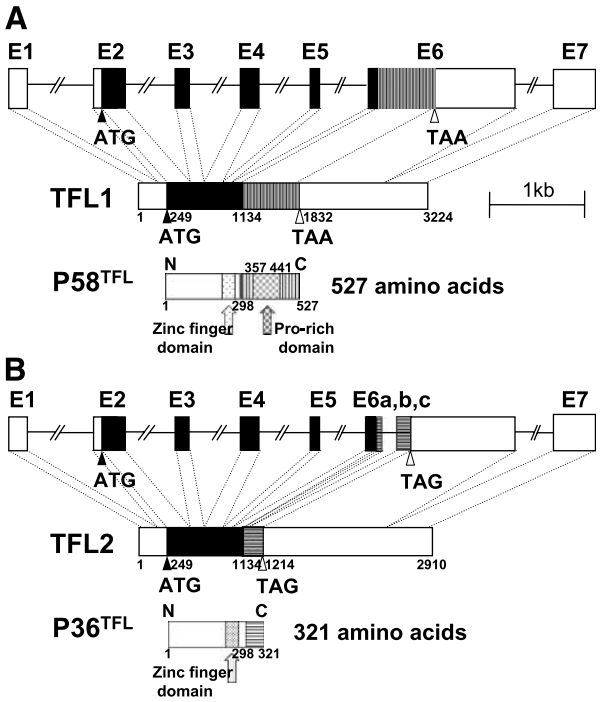

FIGURE 1. Two alternatively spliced gene products. Exon organizations of two transcripts, TFL1 (**A**) and TFL2 (**B**), are illustrated at the top. The GenBank/EMBL/DDBJ Data Bank accession numbers of TFL1 and TFL2 are #AB458221 and #AB458222, respectively. Exon and intron are indicated by box and line, respectively. Common and unique ORFs are shown by black and gray boxes, respectively. TFL1 and TFL2 encode P58^{TFL} and P36^{TFL}, respectively. P58^{TFL} and P36^{TFL} had a common amino-terminal sequence (*white boxes*) including a CCCH-type zinc finger domain (*dotted box*) and specific carboxyl-terminal sequences (*white box with vertical or horizontal lines*) and a Pro-rich domain (*checked box*).

Results

Identification of Two Alternatively Spliced Transcripts

At the beginning of our cDNA cloning, two independent genes, *ZC3H12D* and "an orphan gene encoding FLJ00361 protein (accession #AK090441)," were listed at the NCBI database. RNA blot analysis using a DNA fragment of the *TFL* gene cloned from a genomic library constructed from a patient's lymph node with t(2;6)(p12;q25) (ref. 22) and a 5.5-kb cDNA clone, FLJ00361, provided by KAZUSA DNA Research Institute (Tsukuba, Japan), supported the possibility that *TFL* was composed of the putative two independent genes described above (data not shown). Thereafter, we identified two alternatively spliced 3.2- and 2.9-kb cDNAs, designated TFL1 and TFL2 (Fig. 1).

The 3.2-kb TFL1 cDNA was composed of 7 exons, and a predicted open reading frame (ORF) of 1,584 bp encodes a 527-amino-acid protein. It has a 249-bp 5′ untranslated region (5′UTR) and a 1,392-bp 3′UTR (Fig. 1A). The 2.9-kb TFL2 cDNA had the identical exons 1 to 5 and exon 7 of TFL1, but exon 6 was subdivided into three exons, 6a, 6b, and 6c, by alternative splicing (Fig. 1B). Consequently, a frame shift occurs in the ORF of TFL2, resulting in a stop codon TAG at nucleotide number 1214. Thus, the ORF of TFL2 is 966 bp, encoding 321 amino acids, of which the last 23 amino acids are distinct from the carboxyl 229-residue sequence of TFL1 (Fig. 1B). The predicted primary structures include a common CCCH-type zinc finger domain and a proline-rich domain in TFL1. No other known motifs were found.

The cDNA sizes were smaller than the major transcript size, 5 kb, determined by RNA blot analysis of human lymphocytes (Fig. 2A). In light of this, we also screened a cDNA library derived from human peripheral blood by plaque hybridization using a common cDNA fragment of exon 6. However, only cDNAs possessing the same boundary between exon 6 and exon 7 with a poly A$^+$ tail were identified. Thus, we speculate that the 5′UTR of the major transcript is longer than those of the smaller transcripts, or alternatively, it is possible that exons 6 and 7 are not spliced in the major pre-mRNA. In fact, the FLJ00361 5.5-kb cDNA lacking a large part of the ORF in TFL1 or TFL2 has a long intron 6 sequence.

Expression Profiles in Normal Tissues and Leukemic Cell Lines

We first examined mRNA expression in human blood to gain insight about the functional significance of *TFL* in malignant lymphoma (Fig. 2A). The 5-kb *TFL* transcript was abundantly expressed in human lymph nodes as well as in normal peripheral T and B lymphocytes. In contrast, human bone marrow expressed less of this transcript. Human B-cell (Daudi and Nalm6) and some myeloid leukemia/lymphoma cell lines (THP-1) expressed *TFL* as well as did lymph nodes. However, it was less abundant in another myeloid leukemic cell line, HL60. In contrast, mRNA expression in T-cell leukemia/lymphoma cell lines (Jurkat, Molt14, and CCRF/CEM) was undetectable. A smaller transcript (~3.2 kb) was also seen in THP-1 and Daudi cells, which was compatible in size with our cDNA clone TFL1.

We next examined mRNA expression in other normal tissues. The 5-kb transcript was prominently expressed in mouse lymphoid organs, spleen, and thymus (Fig. 2B, *left*). The mRNA was also detectable in lung, stomach, and kidney, whereas it was undetectable in brain, heart, liver, and muscle. Mouse *TFL* was also expressed in both splenic T and B lymphocytes (Fig. 2B, *right*). Although the transcript was not detectable in mouse bone marrow, a faint expression was seen not only in the mouse pro-B-cell line Ba/F3 but also in the myeloid progenitor cell line 32D.

These results indicate that *TFL* is predominantly expressed in normal lymphoid tissues and that some lymphoid malignancies lack expression.

Identification of the Major Protein Expressed in Human Blood

We next confirmed the expression of *TFL*-encoded protein by developing polyclonal antisera against recombinant protein derived from a TFL2 cDNA expression vector. As shown in Fig. 1, the first 298 amino acids encoded by TFL1 are identical to those of TFL2. Thus, the antisera could recognize a 58-kDa protein, P58^{TFL}, in Ba/F3 cells transfected with a TFL1 expression vector (Fig. 3A). P58^{TFL} was preferentially expressed in human peripheral mononuclear cells (MNC) but not in polymorphonuclear cells (PMN). The expression pattern in human

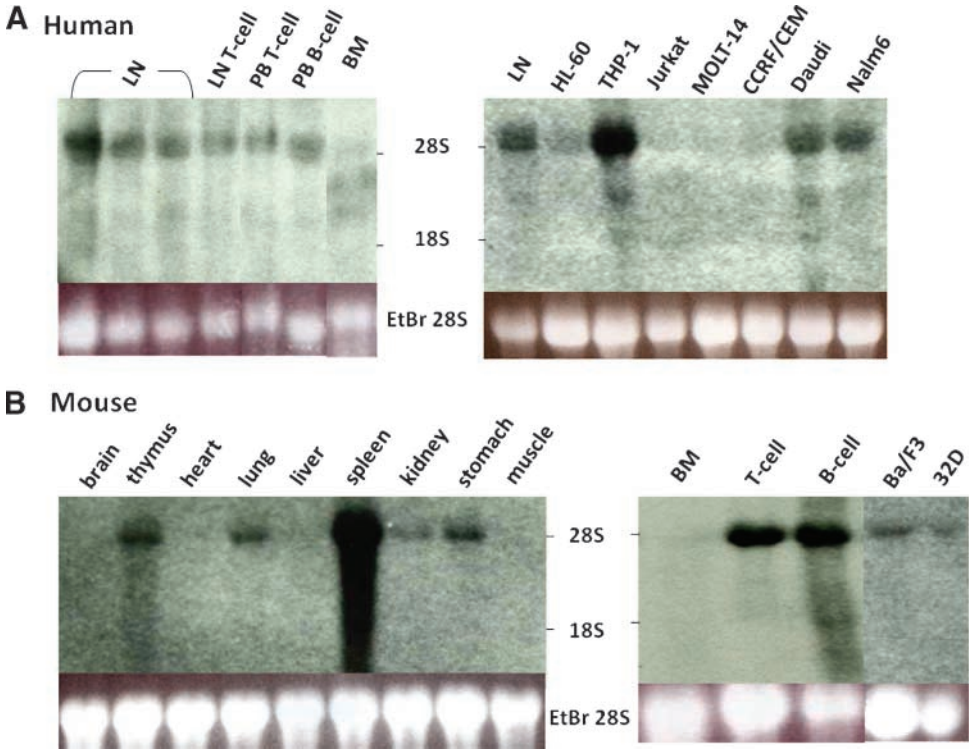

FIGURE 2. Tissue-specific mRNA expression. **A.** RNA blots of normal human lymph nodes (*LN*), peripheral blood (*PB*) T and B lymphocytes, and bone marrow (*BM*; *left*) and human leukemia/lymphoma cell lines (HL-60, THP-1, Jurkat, Molt-14, CCRF/CEM, Daudi, and Nalm6) were probed with a human cDNA fragment covering the common ORF of TFL1 and TFL2. The positions of 28S and 18S rRNAs are shown. Ethidium bromide (*EtBr*) staining of 28S rRNA is also shown at the bottom of the blots. **B.** RNA blots of normal mouse tissues (*left*) and mouse bone marrow, splenic T and B lymphocytes, IL-3–dependent pro-B cell line, Ba/F3, and myeloid progenitor cell line, 32D (*right*), were probed with mouse cDNA.

hematopoietic cell lines was completely consistent with the results of RNA blot analyses (Figs. 2A and 3A).

To further confirm the specificity of the antisera, we performed immunoblot analysis using immunoprecipitates. The $P58^{TFL}$ was specifically immunoprecipitated, but a nonspecific signal (indicated by a star just above $P58^{TFL}$) that was detected in cell lysates was absent (Fig. 3). With regard to protein encoded by TFL2, the antisera could recognize recombinant $P36^{TFL}$ expressed in a mammalian cell line (Fig. 3B). Both molecular weights (MW) observed experimentally by SDS-PAGE analysis were compatible with those predicted from their primary structures. $P36^{TFL}$ seems to be similar to a provisionally named p34, although there is a four-amino-acid difference from codon 298 to codon 301 (P34, Pro-Val-Leu-Pro; $P36^{TFL}$, Leu-Gly-Val-Arg, respectively) by possible alternative splicing of exons 6a and 6b (23). However, the endogenous $P36^{TFL}$ was

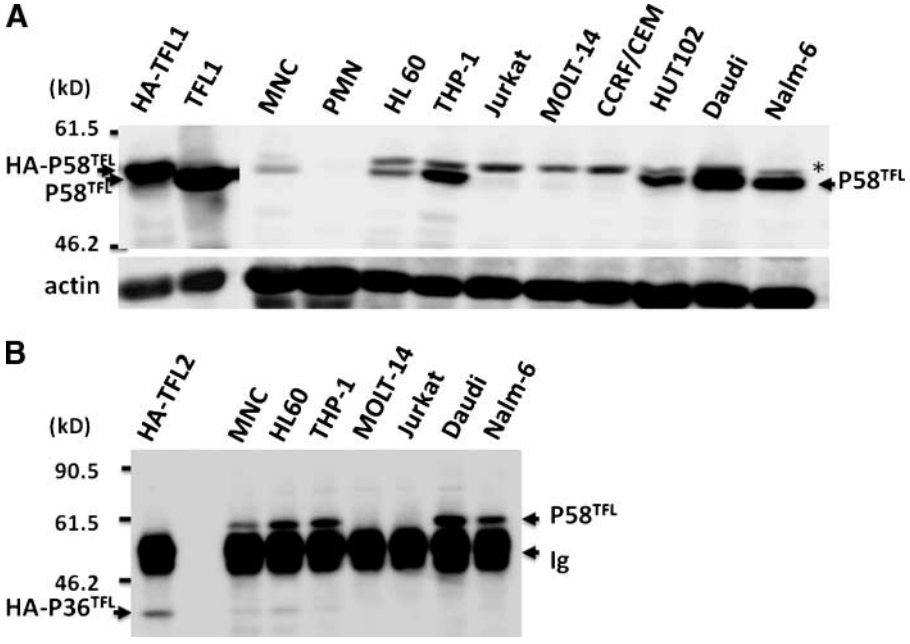

FIGURE 3. Dominant expression of $P58^{TFL}$ in human blood cells. Immunoblot analyses of human TFL in human normal WBC and leukemia cell lines. Total cell lysates of HA-tagged or nontagged TFL1 cDNA transfectants, HA-TFL1 and TFL1 (**A**), and immunoprecipitates of HA-tagged TFL2 cDNA transfectants, HA-TFL2, were used as controls of recombinant $P58^{TFL}$ and $P36^{TFL}$, respectively. In addition to the cell lines for RNA blot analysis (Fig. 2), a mature T-cell lymphoma cell line, HUT102, was also examined. The MW of major TFL protein was 58 kDa (**A**). A nonspecific signal (*) was absent from immunoprecipitated samples (**B**).

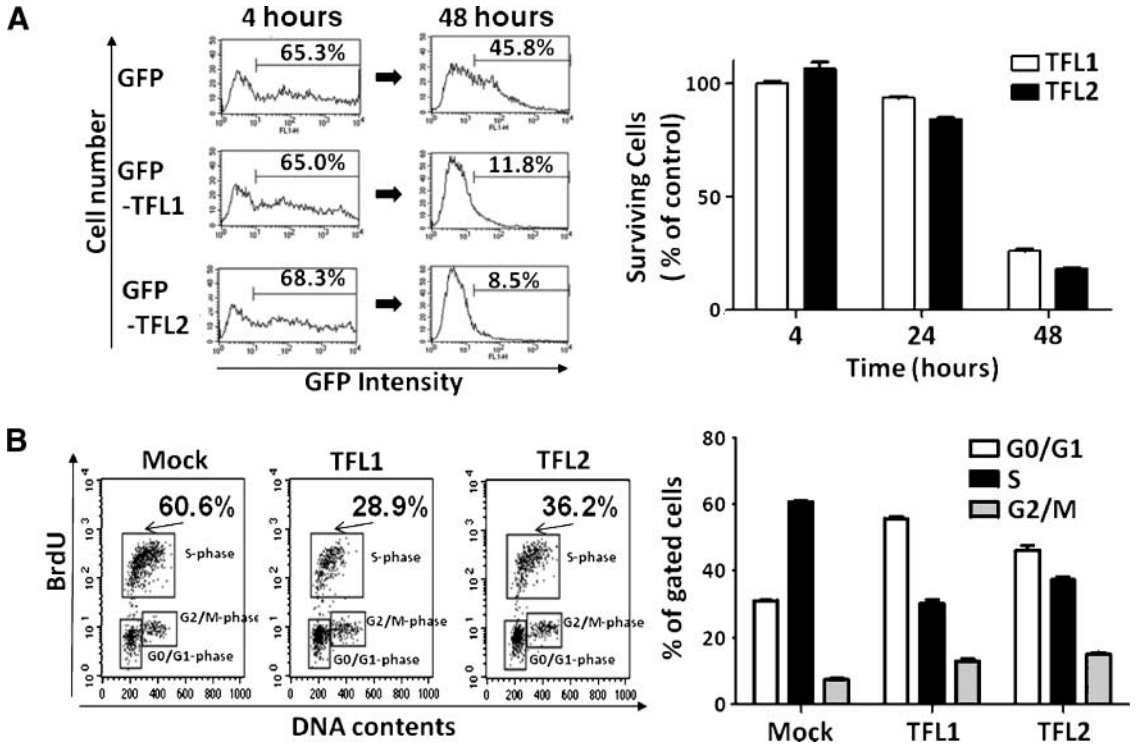

FIGURE 4. TFL interfered with progression to S phase. **A.** Ba/F3 cells were nucleofected with vectors containing GFP-tagged mock or TFL1 or TFL2 cDNA. GFP-positive cells were analyzed by flow cytometry at 4, 24, and 48 h after electroporation. Left, representative cytograms at 4 and 48 h. The bar graph shows time-dependent decreases of GFP-TFL–positive cells. Columns, mean surviving cells (% of control) compared with mock transfectants from three experiments; bars, SD. **B.** Representatives of three independent BrdUrd assays using mock, TFL1, and TFL2 cDNA transfectants (*left*). After IL-3 starvation for 16 h, Ba/F3 transfectants were cultured in the presence of IL-3 for an additional 16 h. Then, cells were assessed for BrdUrd incorporations. The bar graph shows percentages of gated cells in G_0-G_1, S, or G_2-M phase. Columns, mean of triplicate samples; bars, SD.

not evident by immunoblot using whole-cell lysates. Some diffuse bands that comigrated with the recombinant P36^{TFL} in MNC, HL60, and THP-1 immunoprecipitates are not likely to represent endogenous P36^{TFL} because the recombinant P36^{TFL} was tagged with hemagglutinin (HA). Thus, the major protein expressed in normal human lymphocytes was P58^{TFL}. Moreover, aberrant expression of P58^{TFL} was found in some human leukemic cell lines.

TFL Inhibits DNA Synthesis and Progression to S Phase

To clarify the biological function of TFL, a green fluorescent protein (GFP)-TFL fusion protein was expressed in an interleukin 3 (IL-3)–dependent mouse normal pro-B-cell line, Ba/F3, where the *TFL* mRNA expression level was less than that of mature B lymphocytes (Fig. 2B). Interestingly, although the numbers of cells expressing GFP-TFL1 or GFP-TFL2 were equivalent to the number expressing GFP alone at 4 hours after electroporation, the number of cells expressing either TFL1 or TFL2 was drastically decreased by 48 hours (Fig. 4A). We speculated that this might be due to TFL-induced growth arrest and/or cell death because the population of nontransfected Ba/F3 cells soon overwhelmed that of TFL transfectants.

To examine whether TFL could suppress DNA synthesis, we performed bromodeoxyuridine (BrdUrd) assays under G_0-G_1 synchronization conditions as described in Materials and Methods. As expected, the number of S-phase cells incorporating BrdUrd was decreased by introducing TFL1 or TFL2 cDNA (Fig. 4B). The number of G_0-G_1-phase cells among transfectants was increased proportionately. These results indicate that the G_1 to S phase progression was inhibited by TFL. Inhibition of DNA synthesis by TFL was also confirmed by tritiated thymidine uptake (data not shown). The observation that growth inhibition was observed after introducing either TFL1 or TFL2 cDNAs suggests that a common protein domain between P58^{TFL} and P36^{TFL} might play a crucial role in cell growth control.

TFL Suppresses Phosphorylation of Retinoblastoma Protein

Cell cycle progression is regulated by many signaling molecules. Phosphorylation of retinoblastoma protein (Rb) plays a key role in the G_1 to S phase transition (24). To determine whether TFL could inhibit Rb phosphorylation or not, we first assessed Rb phosphorylation status in Ba/F3 transfectants by intracellular flow cytometry assay (Fig. 5A). As expected, introduction of either TFL1 or TFL2 cDNA significantly restrained Rb phosphorylation compared with a control vector alone (mock). These results indicated that TFL inhibited cell cycle progression into S phase through the suppression of Rb phosphorylation. To confirm this finding in another cell line, NIH3T3 cells were transfected with the GFP-tagged TFL vectors. Rb phosphorylation was then assessed by immunofluorescence staining using a specific antibody for phospho-Rb. Cells expressing GFP-TFL1 fusion protein completely lacked Rb phosphorylation

(Fig. 5B, *middle*), although Rb was phosphorylated in the mock-transfected cells (Fig. 5B, *top*). Similar results were found in cells expressing P36^{TFL} as well (Fig. 5B, *bottom*).

TFL Promotes Caspase-3–Dependent Apoptosis

Apoptotic pathways are also important for the development of cancers. To examine the effect of TFL on cell apoptosis, Ba/F3 cells carrying TFL vectors were stained with Annexin V. As shown in Fig. 6A, both types of TFL increased the number of Annexin V–positive cells by 24 hours after electroporation. To confirm whether cell death was caspase-3 dependent or not, we also studied the activation of caspase-3 by flow cytometry. Ba/F3 cells carrying TFL1 as well as TFL2 vectors had significantly increased cleaved caspase-3 compared with mock transfectants (Fig. 6B). These results suggest that both P58^{TFL} and P36^{TFL} induced caspase-3–dependent apoptosis.

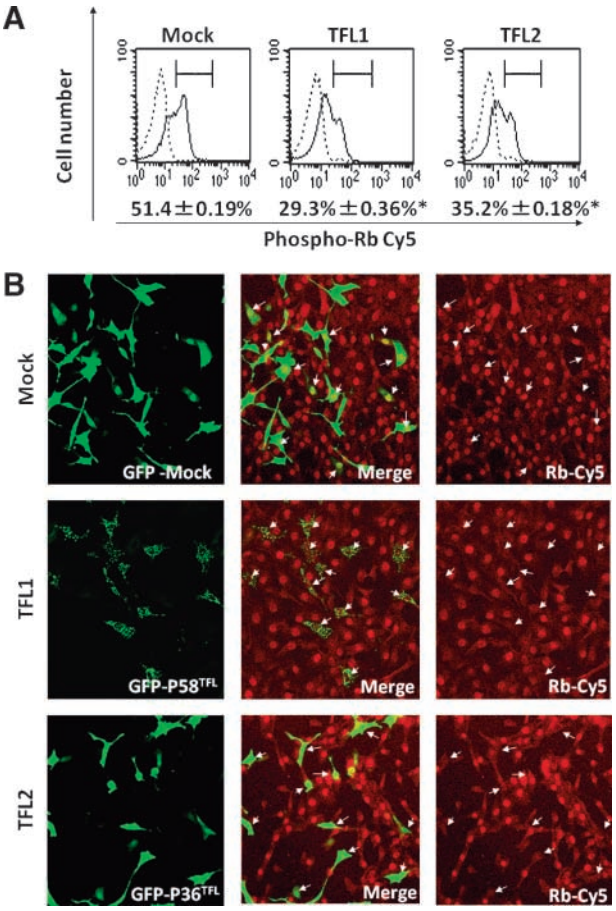

FIGURE 5. TFL suppressed Rb phosphorylation. **A.** Phosphorylation levels of Rb in GFP-positive Ba/F3 cells were analyzed by intracellular flow cytometry using Cy5-conjugated phospho-Rb–specific antibody. Dashed lines, isotype control. *, $P < 0.01$, phospho-Rb–positive cells in TFL1 and TFL2 transfectants compared with mock transfectants. Results are expressed as mean ± SD of triplicate samples. **B.** Immunofluorescence staining of phospho-Rb for NIH3T3 cells transfected with designated GFP fusion vectors. Almost all Rb proteins of control transfectants (Mock GFP-positive cells indicated by arrows) were phosphorylated as shown as yellow nuclei in a merged panel, whereas TFL1 and TFL2 transfectants indicated by arrows showed less Rb phosphorylation as shown as faint red nuclei in Rb-Cy5 staining in both transfectants. There are no yellow signals in the merged image of TFL2.

Overexpression of TFL Alters the Caricinogenic Properties of Human Leukemia Cells

It is interesting that the predominant lymphocytic splice form, TFL1, was not expressed in certain human leukemia cell lines as described above (Fig. 3A). To examine whether the deficiency is only correlative or causative for leukemogenisis, we tried some functional assays by introducing the *TFL* cDNA expression vectors into the T-cell leukemia cell line Jurkat.

Overexpression of TFL1 as well as TFL2 inhibited the growth of Jurkat cells (Fig. 7A). Moreover, TFL vectors suppressed BrdUrd incorporation and Rb phosphorylation, and it increased cleaved caspase-3–positive apoptotic cells (Fig. 7B–D). These results indicate that TFLs serve as a tumor suppressor in certain human leukemia cells.

Differential Subcellular Localization of P58^{TFL} and P36^{TFL}

We also examined the subcellular localization of P58^{TFL} and P36^{TFL} (Fig. 8A). P58^{TFL} localized as discrete granules in the cytoplasm, but not at all in the nuclei, of HeLa cells. On the other hand, P36^{TFL} localized to both cytoplasm and nuclei (but not nucleoli); nuclei were stained more intensely than the cytoplasm. The distinctive localization of P58^{TFL} and P36^{TFL} was confirmed in NIH3T3 and Ba/F3 transfectants (data not shown). There are some differences in the carboxyl-terminal sequences between P58^{TFL} and P36^{TFL} (Fig. 1). These differences may contribute to specific subcellular localization through as yet unidentified sequence motifs present within this region.

TFL has a single CCCH-type zinc finger motif that binds nucleic acids including RNA. mRNA processing bodies (P-bodies), where mRNA degradation or stabilization occurs, are localized to the cytoplasm as discrete granules. We predicted that P58^{TFL} granules might colocalize with P-bodies. Thus, we cotransfected GFP-tagged P58^{TFL} with HA-tagged P-body markers, eukaryotic translation initiation factor 2C (EIF2C2; also known as AGO2; ref. 25) or DCP1 decapping enzyme homolog A (DCP1A; ref. 26). Almost complete colocalization of P58^{TFL} and EIF2C2 was confirmed in the transfectants (Fig. 8B, *top*). DCP1A signals also colocalized within P58^{TFL} granules. Some P58^{TFL} green granules lack DCP1A red signals because the latter were less expressed than P58^{TFL}.

Both P-bodies and stress granules are distinct cytoplasmic aggregates involved in mRNA storage and/or degradation, but they are spatially, compositionally, and functionally linked (27, 28). It is possible that P58^{TFL} might be also accumulating in foci near P-bodies much like stress granules. Therefore, we further examined the subcellular localization by cotransfection with a HA-tagged stress granule marker, T-cell intracellular antigen-1 (TIA-1; Fig. 8B, *bottom*). Most P58^{TFL} and TIA-1 granules are distinctively localized in the cytoplasm. A few P58^{TFL} granules were juxtaposed with TIA-1 granules, but the two granules never overlapped. Interestingly, overexpression of mouse TFL in HeLa cells promoted the fusion of endogenous TIA-1–positive stress granules with TFL granules. Some stress granules were incompletely engulfed by TFL (Supplementary Fig. S1). In contrast, other granules such as endosomes or lysosomes were not colocalized with P58^{TFL} granules, as assessed with anti-EEA1 antibody and LysoTracker, respectively (refs. 29, 30; data not shown).

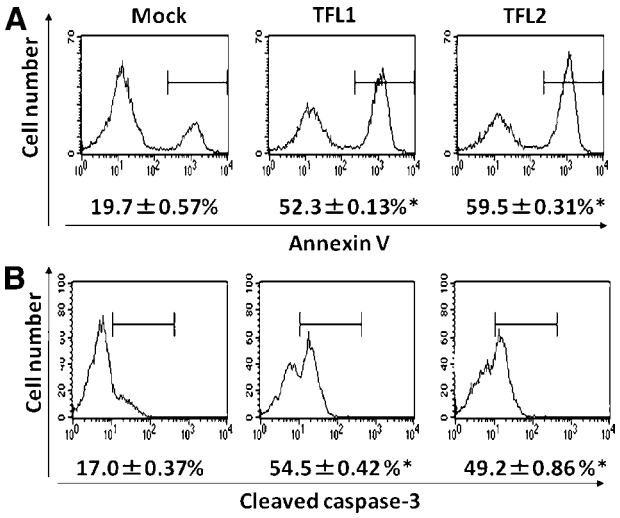

FIGURE 6. Apoptosis induced by TFL. **A.** Ba/F3 transfectants of mock, GFP-TFL1, and GFP-TFL2 cDNA vectors were stained with Annexin V-Cy5 at 24 h after transfection. *, $P < 0.01$, Annexin V–positive cells were significantly increased in GFP-positive TFL1 and TFL2 transfectants versus mock. Results are expressed as mean ± SD of triplicate samples. **B.** Representatives cleaved caspase-3–positive cell analyses. *, $P < 0.01$, percentages of active caspase-3–positive cells in GFP-positive TFL1 or TFL2 transfectants compared with that in mock transfectants (GFP alone). Results are expressed as mean ± SD of triplicate samples.

These results suggest that P58^{TFL} may be a component of the P-body, which spatially interacts with stress granules and might suppress G_1 to S phase progression through posttranscriptional modification of an indispensable cell cycle regulator.

Discussion

ZC3H12D belongs to a gene family including three other members, *ZC3H12A, ZC3H12B*, and *ZC3H12C*. Among them, monocyte chemoattractant protein-1–induced protein (*MCPIP*) was first identified as a product of *ZC3H12A* in monocyte chemoattractant protein-1–activated monocytes (31). *ZC3H12B* and *ZC3H12C* mRNAs were expressed in normal tissues with unique expression profiles,[1] but their expression at the protein level has not yet been confirmed. Here, we first identified two *ZC3H12D*-derived splicing variants encoding possible tumor suppressors, P58^{TFL} and P36^{TFL}. In contrast to the dominant expression of *ZC3H12A* in macrophages, *ZC3H12D* was expressed preferentially on normal lymphoid tissues. In particular, it was very strongly expressed on mature T and B lymphocytes rather than immature thymocytes. Whereas TFL^{p58} was undetectable in some immature hematopoietic cell lines such as Jurkat, MOLT-14, and CCRF/CEM, the mature adult T-cell leukemia cell line HUT102 expressed it intensively (Fig. 2A). MCPIP is inducible in macrophages by inflammatory stimuli, such as lipopolysaccharide, and regulates proinflammatory activation of macrophages by a negative feedback loop (32). A prototype CCCH-type zinc finger protein, tristetraprolin, encoded by the *Zfp36* gene, also regulates tumor necrosis factor α in macrophages through a negative feedback loop (33). Therefore, TFL proteins might play some feedback roles in lymphocyte activation as well as maturation. It is of interest how P58^{TFL} and P36^{TFL} are regulated under T-cell receptor or Ig stimulus.

We originally identified the *TFL* gene *ZC3H12D* by cloning the breakpoint of a t(2;6)(p12;q25) translocation in a BCL-2–positive transformed follicular lymphoma (22). The 5′ region of *ZC3H12D* including exon 1 and exon 2 was replaced by the Vκ and Cκ regions of the *Igκ* gene. Originally, another 6q allele had been lost in the follicular lymphoma before the transformation. However, it remains to be elucidated whether deregulation of the gene or deletion is relevant to transformation. The growth inhibitory activities of P58^{TFL} and P36^{TFL} on a human leukemia cell line shown here support the hypothesis that loss of the biological function by translocation is implicated in transformation as a tumor suppressor. Deregulated antiapoptotic protein BCL-2, preventing cellular apoptosis in follicular lymphoma, causes massive lymphoid hyperplasia, a premalignant state (34, 35). A secondary hit at *ZC3H12D* in lymphocytes might result in complete loss of their normal function, facilitating a release from the growth control into tumor progression. Moreover, loss of heterozygosity of *ZC3H12D* was found in sporadic lung cancer, whereas normal lung expressed the mRNA. By using a human lung carcinoma cell line, Wang et al. (23) showed that a single amino acid change due to single-nucleotide polymorphism contributes to tumor progression. However, there was no significant difference in the growth inhibition between mouse pro-B-cell lines overexpressing TFL with an exchanged codon at 106, from lysine to arginine, according to the single-nucleotide polymorphism (data not shown). Whether this discrepancy is due to the cell lines used or reflects different tissue specificity is not yet clear. In addition, the four-amino-acid difference between p34 and P36^{TFL} might affect biological activity.

Suppression of Rb phosphorylation is thought to precede G_0-G_1 arrest in P58^{TFL} and P36^{TFL} transfectants. Activated cyclin-dependent kinase phosphorylates multiple sites in Rb, and phosphorylated Rb up-regulates cell growth–related proteins (36). Microarray screening of the expression profiles of cell cycle–related genes in the transfectants revealed the down-regulation of *PCNA, E2F3*, and *E2F4*, as expected.[2] Just as MCPIP could contribute to the suppression of tissue inflammation, TFL also might prevent from excessive lymphocyte proliferation following tissue damage, an origin of cancer development.

MCPIP is reported to induce apoptosis in monocytes as well as in cardiac myocytes (37). In addition to G_0-G_1 arrest, caspase-3–dependent apoptosis was confirmed in Ba/F3 cells overexpressing P58^{TFL} or P36^{TFL}. There are two possibilities about how apoptosis was induced in the transfectants. First, TFL may directly promote apoptosis through a different signaling pathway from that inducing G_0-G_1 arrest. Alternatively, it may be possible that cell cycle arrest caused apoptosis in the

[1] Unpublished observations.

[2] Unpublished observation.

transfectants. It is meaningful to determine whether or not the apoptosis is induced in a p53-dependent manner because p53 is involved in cell cycle arrest as well as apoptosis. Apoptosis is characterized by chromatin condensation, internucleosomal degradation of the DNA, cell shrinkage, and disassembly into membrane-enclosed vesicles as a consequence of caspase-3 activation (38). Because apoptosis is generally accompanied by a reduction in cell volume, this parameter was used to discriminate between morphologically apoptotic and viable cell populations (39). Thus, we examined cell cycles as well as Rb phosphorylation by discerning such shrinkage, so-called morphologically apoptotic cells, with flow cytometry. Indeed, cleaved caspase-3–positive cells were not increased in morphologically viable cell populations at all (data not shown). In addition, the number of apoptotic cells accumulated in a time-dependent manner. These results suggest that G_0-G_1 arrest preceded apoptosis in Ba/F3 transfectants.

Thus far, no differences in the biological functions of $P58^{TFL}$ and $P36^{TFL}$ have been found. However, their subcellular distributions were distinctive. $P58^{TFL}$ was shown to be colocalized with P-body–related proteins, EIF2C2 and DCP1A. Posttranscriptional mechanisms are gradually becoming better defined and are gaining attention (40). For example, EIF2C2 is a major RNA-induced silencing complex component where microRNA as well as short interference RNA is processed. RNA-induced silencing complex components play an important role for posttranscriptional pathways (25, 41). In addition to mRNA processing, sites for mRNA editing are very unique. When cellular stress triggers mRNA processing, mRNA and RNA binding proteins are gathered in cytoplasmic granules called P-bodies and stress granules (42). The tandem CCCH-type zinc finger domain originally identified in tristetraprolin binds to AU-rich elements, regulating mRNA stability (33). A similar zinc finger domain–containing protein, Roquin, was also shown to be an RNA-binding protein localized in P-bodies (43, 44). Recent surveys indicate that posttranscriptional pathways and mRNA processing pathways are indispensable to the regulation of protein expression as well as its deregulation in tumorigenesis. With this in mind, $P58^{TFL}$ might bind to certain RNA AU-rich elements and be involved in posttranscriptional modification. More comprehensive assays will be required to identify target molecules of $P58^{TFL}$ and define its role as an RNA binding protein.

In contrast, MCPIP is thought to work as a transcription factor (45). Similarly, $P36^{TFL}$ contains the same zinc finger domain and might be a transcriptional factor because of its unique localization in the nucleus but not nucleoli. The identification of molecular targets of $P58^{TFL}$ and $P36^{TFL}$ would help address the question of how these proteins control cell cycle and apoptosis.

The data presented here show that $P58^{TFL}$ and $P36^{TFL}$ regulate cell growth likely by suppressing Rb phosphorylation. Although future studies are needed to ascertain whether the deregulation $P58^{TFL}$ and/or $P36^{TFL}$ is actually involved

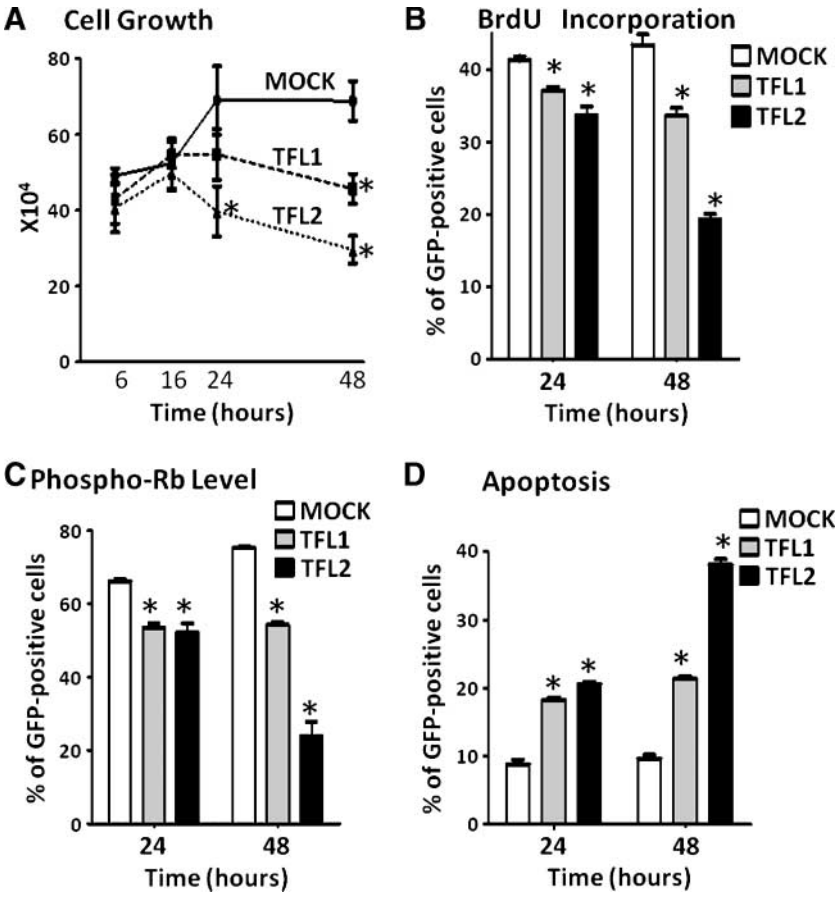

FIGURE 7. Overexpression of TFL alters the leukomogenic properties of Jurkat cells. **A.** Human T-cell leukemia Jurkat cells (5×10^5) were nucleofected with vectors containing GFP-tagged mock, TFL1, or TFL2 cDNA vectors. GFP-positive cells were analyzed by flow cytometry at 6, 16, 24, and 48 h after electroporation. Living cell numbers were counted by trypan blue method. Representative cell growth curves of transfectants. *, $P < 0.01$, GFP-positive cells in TFL1 and TFL2 transfectants compared with mock transfectants. Points, mean of triplicate samples; bars, SD. **B.** Jurkat cells overexpressing TFLs were cultured for 24 and 48 h to assess for BrdUrd incorporations. Representatives of three independent BrdUrd assays using mock, TFL1, and TFL2 cDNA transfectants. The bar graph shows percentage of GFP-positive cells in S phase. *, $P < 0.01$, BrdUrd-positive cells in TFL1 and TFL2 transfectants compared with mock transfectants. Columns, mean of triplicate samples; bars, SD. **C.** Phosphorylation levels of Rb in Jurkat cells overexpressing TFL1 or TFL2 were analyzed by intracellular flow cytometry using Cy5-conjugated phospho-Rb–specific antibody. *, $P < 0.01$, phospho-Rb–positive cells in TFL1 and TFL2 transfectants compared with mock transfectants. Columns, mean of triplicate samples; bars, SD. **D.** Increased apoptosis was shown in Jurkat cells overexpressing TFLs. *, $P < 0.01$, percentage of active caspase-3–positive cells in GFP-positive TFL1 or TFL2 transfectants compared with mock transfectants. Columns, mean of triplicate samples; bars, SD.

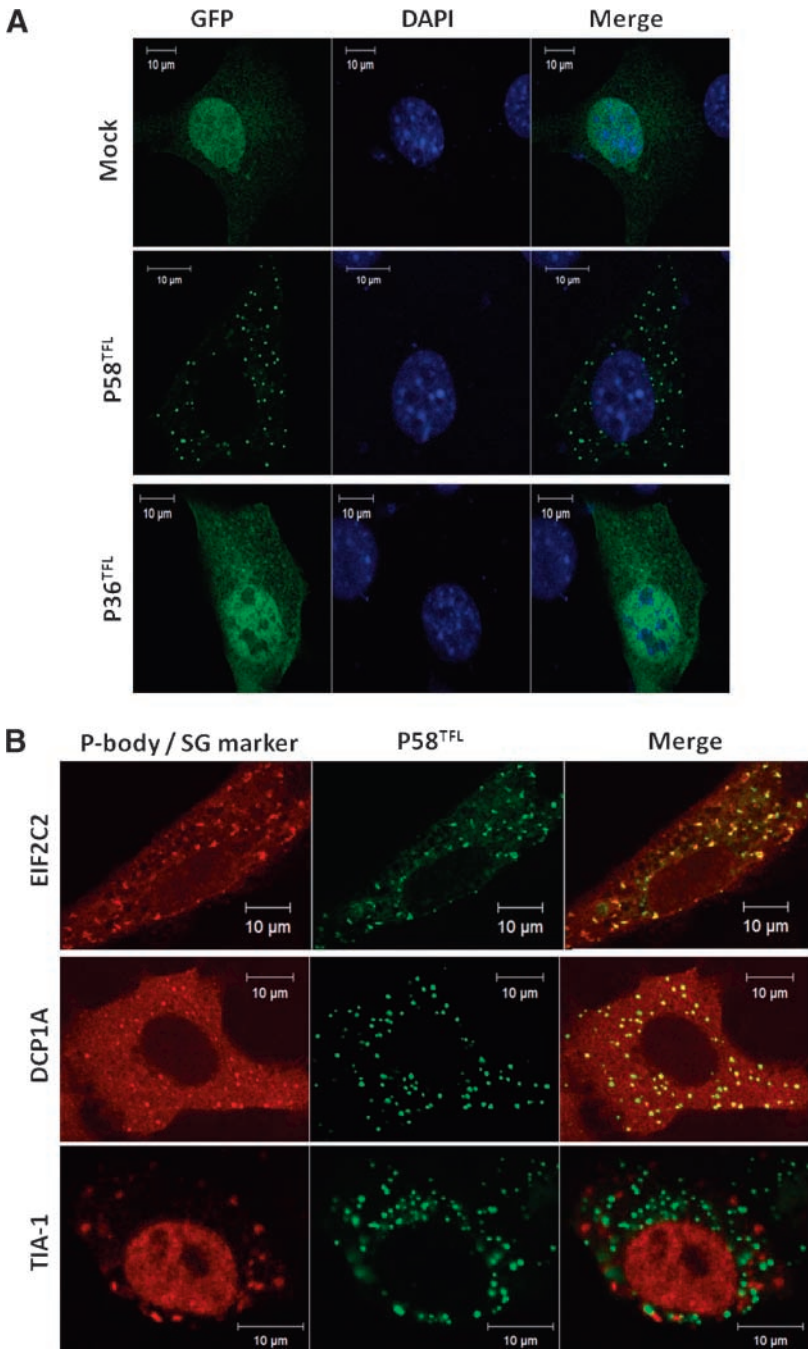

FIGURE 8. Distinct subcellular localization of P58^{TFL} and P36^{TFL}. **A.** Each expression vector of GFP alone or GFP-fused P58^{TFL} or P36^{TFL} was transfected into HeLa cells. Cell nuclei are stained with 4′,6-diamidino-2-phenylindole (*DAPI*). **B.** HA-tagged EIF2C2, DCP1A, or TIA-1 vector was cotransfected with a GFP-fused P58^{TFL} vector into HeLa cells. HA-tagged P-body and stress granule markers were visualized with Cy5-conjugated antibody.

in tumor progression *in vivo*, it is of interest to study their potential utility as diagnostic as well as potential therapeutic targets in various malignancies.

Materials and Methods

Human cDNA Cloning

RNAs were extracted from human lymph nodes with Trizol (Invitrogen). After DNase I digestion, cDNA was prepared using PrimeScript RTase (Takara, Japan). PCR was done with high-fidelity PrimeSTAR HS DNA Polymerase (Takara) using several primer sets designed using the NCBI database. Sequencing of PCR products was done using an ABI PRISM 310 Genetic Analyzer (Applied Biosystems). PCR using just one primer set showed several bands, and sequence analyses showed at least two patterns of splice variants. To clone the TFL1 and TFL2 human cDNAs into expression vectors, the following primer sets were used: a common forward primer, 5′-ATGGAGCACCCCAGCAAGAT-3′, and reverse primers for TFL1, 5′-TTAGGGCTTGCCCAGGGGCGCCC-3′, and TFL2, 5′-CTAGGGCGGTGTTCGCCCCGCGG-3′. To confirm the 3′UTR, we also screened a cDNA library from human peripheral blood (Clontech).

Cells

Ba/F3 and 32D mouse cell lines were maintained in RPMI 1640 containing 10% FCS (JRH Biosciences) and 15% WEHI-conditioned medium (46). Leukemia cell lines, HL-60, THP-1, Jurkat, MOLT-14, CCRF-CEM, HUT102, Daudi, and NALM-6, were maintained in suspension culture using RPMI 1640 containing 10% FCS (47). NIH3T3 and HeLa cells were maintained in DMEM containing 10% calf bovine serum.

Human and mouse T and B lymphocytes (MNC) were isolated by Dynabeads using specific monoclonal antibodies (Dynal Biotech). Mononuclear and polymorphonuclear cells were isolated by Lympholyte-H (Cedarlane) and Histopaque-1119 (Sigma).

RNA Blot Analyses

RNA blots were hybridized with ^{32}P-labeled human and mouse TFL cDNA probes. A 963-bp human TFL probe, which includes the complete ORF of TFL2, was amplified using a forward primer, 5′-ATGGAGCACCCCAGCAAGATGGAATTC-3′, and a reverse primer, 5′-CTACCCACCATAAGGACAATGCTGC-3′. A 600-bp mouse cDNA probe, which includes the homologous region of human TFL2 cDNA ORF, was amplified from mouse spleen lymphocyte RNA using a forward primer, 5′-ATGAGCCATGGAAATAAAGAAGCCT-3′, and a reverse primer, 5′-ACCCAGCCAGGCCCGCGTCTTGGCA-3′.

Antisera

Antihuman TFL polyclonal antibody was generated by immunization of rabbits with glutathione *S*-transferase (GST) fusion protein containing full-length P36^{TFL} (Operon). A GST-P36^{TFL} expression vector was constructed using the pGEX-2TL vector (Amersham Biosciences). Crude rabbit serum was purified with a recombinant TFL protein, GST-P36^{TFL}, affinity column.

Expression Vectors and Transfection

Mammalian cell expression vectors containing human TFL1 and TFL2 cDNAs were constructed by using a pQBI25 GFP vector (Takara, Japan). Each cloned cDNA including its complete ORF was introduced using the *Nhe*I site of the vector. HA-tagged vectors were produced by linker ligation of oligonucleotides, 5′-CTAGATACCCTTATGATGTTCCTGACTATGCCG-3′ and 5′-CTAGCGGCATAGTCAGGAACATCATAAGGGTAT-3′, using the *Nhe*I site of pQBI25 vector. *EIF2C2, DCP1A*, and *TIA-1* cDNAs including complete ORF were ligated into the HA-tagged vector described above using the *Xba*I site.

A mouse TFL cDNA was cloned by reverse transcription-PCR using total RNA of splenocytes and a forward primer, 5′-GCTCGAGATGAGCCATGGAAATAAAGA-3′, and a reverse primer, 5′-CTAAGGATCCCCCAACGGAGC-3′. The mouse cDNA was ligated into the *Xho*I and *Bam*HI sites of a DsRed monomer vector (Clontech).

Ba/F3 cells were electroporated with the Nucleofector system (Amaxa). Adherent cell lines were transfected with Lipofectamine 2000 (Invitrogen) following the manufacturer's protocols.

Immunoblot Analysis

Cells were lysed in lysis buffer containing 50 mmol/L Tris-HCl (pH 7.5), 150 mmol/L NaCl, 0.5% NP40, 1 mmol/L sodium vanadate, 50 mmol/L sodium fluoride, protease inhibitor cocktail (Sigma), and 1 mmol/L phenylmethylsulfonyl fluoride. For immunoprecipitation, total cell lysates were incubated with antihuman TFL antisera, followed by the addition of protein G-Sepharose (Amersham Biosciences), on a rotating shaker for 4 h at 4°C. The immunoprecipitates were washed thrice with lysis buffer and thrice with PBS.

Total cell lysates as well as immunoprecipitates were separated on 10% SDS-polyacrylamide gels and transferred onto polyvinylidene difluoride membranes (Millipore). The membranes were first incubated with TBST [20 mmol/L Tris-HCl (pH 7.5), 150 mmol/L NaCl, 0.1% Tween 20] containing 5% nonfat dried milk and probed with antihuman TFL or rabbit anti–β-actin (Sigma), followed by incubation with secondary horseradish peroxidase. Blots were visualized by enhanced chemiluminescence (Millipore).

BrdUrd, Phospho-Rb, and Apoptosis Assays

For BrdUrd assays, Ba/F3 cells were synchronized in G_0-G_1 phase by IL-3 deprivation for 16 h (48). After TFL expression vectors were introduced, the cells were incubated in complete medium supplemented with IL-3 for an additional 16 h, and the BrdUrd incorporation was assayed using the APC BrdU Flow Kit (Becton Dickinson).

For flow cytometric analyses of phospho-Rb, cells were fixed with 4% formaldehyde and permeabilized with 90% methanol, and then incubated with rabbit anti-mouse serine 807/811 phosphorylated Rb (Cell Signaling Technology) followed by incubation with antirabbit secondary antibody conjugated with Cy5 (Jackson ImmunoReserch).

Annexin V-Cy5 (Becton Dickinson), biotinylated anti–active caspase-3 (Becton Dickinson), and streptavidin-allophycocyanin (e-Biosciences) were used to evaluate cell apoptosis.

Immunofluorescence Staining

Cells were grown on eight-chamber slides (Nunc). After transfection with TFL vectors, cells were fixed with 4% formaldehyde and permeabilized with 0.3% Triton X-100. After blocking procedures, cells were incubated with mouse anti-HA antibody (Covance) overnight at 4°C followed by incubation with antimouse secondary antibody conjugated with Cy5 (Jackson ImmunoReserch) before mounting. For detection of endogenous human TIA-1, we used anti–TIA-1 antibody (Santa Cruz) and secondary antibody conjugated with Alexa488 (Molecular Probes). Fluorescence was analyzed by confocal microscopy (510META, Carl Zeiss).

Statistical Analysis

Student's *t* test was used for comparisons of numerical values in cell growth and apoptosis assays.

Disclosure of Potential Conflicts of Interest

No potential conflicts of interest were disclosed.

Acknowledgments

We thank Dr. Donald P. Bottaro for critical review of the manuscript, and Chie Fukui for technical assistance.

References

1. Frohling S, Dohner H. Chromosomal abnormalities in cancer. N Engl J Med 2008;359:722–34.

2. Licht JD, Sternberg DW. The molecular pathology of acute myeloid leukemia. Hematol Am Soc Hematol Educ Program 2005;137–42.

3. Kuppers R. Mechanisms of B-cell lymphoma pathogenesis. Nat Rev Cancer 2005;5:251–62.

4. Delattre O, Zucman J, Plougastel B, et al. Gene fusion with an ETS DNA-binding domain caused by chromosome translocation in human tumours. Nature 1992;359:162–5.

5. Soda M, Choi YL, Enomoto M, et al. Identification of the transforming EML4-ALK fusion gene in non-small-cell lung cancer. Nature 2007;448:561–6.

6. Rowley JD. Letter: A new consistent chromosomal abnormality in chronic myelogenous leukaemia identified by quinacrine fluorescence and Giemsa staining. Nature 1973;243:290–3.

7. Goldman JM, Melo JV. Chronic myeloid leukemia—advances in biology and new approaches to treatment. N Engl J Med 2003;349:1451–64.

8. Rowley JD. Chromosome studies in the non-Hodgkin's lymphomas: the role of the 14;18 translocation. J Clin Oncol 1988;6:919–25.

9. Horsman DE, Gascoyne RD, Coupland RW, Coldman AJ, Adomat SA. Comparison of cytogenetic analysis, southern analysis, and polymerase chain reaction for the detection of t(14; 18) in follicular lymphoma. Am J Clin Pathol 1995;103:472–8.

10. Bende RJ, Smit LA, van Noesel CJ. Molecular pathways in follicular lymphoma. Leukemia 2007;21:18–29.

11. Zhang Y, Matthiesen P, Siebert R, et al. Detection of 6q deletions in breast carcinoma cell lines by fluorescence *in situ* hybridization. Hum Genet 1998;103:727–9.

12. Bailey-Wilson JE, Amos CI, Pinney SM, et al. A major lung cancer susceptibility locus maps to chromosome 6q23-25. Am J Hum Genet 2004;75:460–74.

13. Tilly H, Rossi A, Stamatoullas A, et al. Prognostic value of chromosomal abnormalities in follicular lymphoma. Blood 1994;84:1043–9.

14. Offit K, Parsa NZ, Gaidano G, et al. 6q deletions define distinct clinicopathologic subsets of non-Hodgkin's lymphoma. Blood 1993;82:2157–62.

15. Cheung KJ, Shah SP, Steidl C, et al. Genome-wide profiling of follicular lymphoma by array comparative genomic hybridization reveals prognostically significant DNA copy number imbalances. Blood 2008.

16. Viardot A, Moller P, Hogel J, et al. Clinicopathologic correlations of genomic gains and losses in follicular lymphoma. J Clin Oncol 2002;20:4523–30.

17. Zhang L, Anglesio MS, O'Sullivan M, et al. The E3 ligase HACE1 is a critical chromosome 6q21 tumor suppressor involved in multiple cancers. Nat Med 2007;13:1060–9.

18. Anglesio MS, Evdokimova V, Melnyk N, et al. Differential expression of a novel ankyrin containing E3 ubiquitin-protein ligase, Hace1, in sporadic Wilms' tumor versus normal kidney. Hum Mol Genet 2004;13:2061–74.

19. Cools J, DeAngelo DJ, Gotlib J, et al. A tyrosine kinase created by fusion of the PDGFRA and FIP1L1 genes as a therapeutic target of imatinib in idiopathic hypereosinophilic syndrome. N Engl J Med 2003;348:1201–14.

20. Tefferi A, Vardiman JW. Classification and diagnosis of myeloproliferative neoplasms: the 2008 World Health Organization criteria and point-of-care diagnostic algorithms. Leukemia 2008;22:14–22.

21. Yamamoto K, Okamura A, Minagawa K, et al. A novel t(2;6)(p12;q23) appearing during transformation of follicular lymphoma with t(18;22)(q21;q11) to diffuse large cell lymphoma. Cancer Genet Cytogenet 2003;147:128–33.

22. Minagawa K, Yamamoto K, Nishikawa S, et al. Deregulation of a possible tumour suppressor gene, ZC3H12D, by translocation of IGK@ in transformed follicular lymphoma with t(2;6)(p12;q25). Br J Haematol 2007;139:161–3.

23. Wang M, Vikis HG, Wang Y, et al. Identification of a novel tumor suppressor gene p34 on human chromosome 6q25.1. Cancer Res 2007;67:93–9.

24. Sherr CJ. Cancer cell cycles. Science 1996;274:1672–7.

25. Sen GL, Blau HM. Argonaute 2/RISC resides in sites of mammalian mRNA decay known as cytoplasmic bodies. Nat Cell Biol 2005;7:633–6.

26. Cougot N, Babajko S, Seraphin B. Cytoplasmic foci are sites of mRNA decay in human cells. J Cell Biol 2004;165:31–40.

27. Kedersha N, Stoecklin G, Ayodele M, et al. Stress granules and processing bodies are dynamically linked sites of mRNP remodeling. J Cell Biol 2005;169:871–84.

28. Wilczynska A, Aigueperse C, Kress M, Dautry F, Weil D. The translational regulator CPEB1 provides a link between dcp1 bodies and stress granules. J Cell Sci 2005;118:981–92.

29. Christoforidis S, McBride HM, Burgoyne RD, Zerial M. The Rab5 effector EEA1 is a core component of endosome docking. Nature 1999;397:621–5.

30. Huynh KK, Eskelinen EL, Scott CC, Malevanets A, Saftig P, Grinstein S. LAMP proteins are required for fusion of lysosomes with phagosomes. EMBO J 2007;26:313–24.

31. Liang J, Song W, Tromp G, Kolattukudy PE, Fu M. Genome-wide survey and expression profiling of CCCH-zinc finger family reveals a functional module in macrophage activation. PLoS ONE 2008;3:e2880.

32. Liang J, Wang J, Azfer A, et al. A novel CCCH-zinc finger protein family regulates proinflammatory activation of macrophages. J Biol Chem 2008;283:6337–46.

33. Carballo E, Lai WS, Blackshear PJ. Feedback inhibition of macrophage tumor necrosis factor-α production by tristetraprolin. Science 1998;281:1001–5.

34. McDonnell TJ, Deane N, Platt FM, et al. bcl-2-immunoglobulin transgenic mice demonstrate extended B cell survival and follicular lymphoproliferation. Cell 1989;57:79–88.

35. Nunez G, London L, Hockenbery D, Alexander M, McKearn JP, Korsmeyer SJ. Deregulated Bcl-2 gene expression selectively prolongs survival of growth factor-deprived hemopoietic cell lines. J Immunol 1990;144:3602–10.

36. Knudsen ES, Wang JY. Dual mechanisms for the inhibition of E2F binding to RB by cyclin-dependent kinase-mediated RB phosphorylation. Mol Cell Biol 1997;17:5771–83.

37. Zhou L, Azfer A, Niu J, et al. Monocyte chemoattractant protein-1 induces a novel transcription factor that causes cardiac myocyte apoptosis and ventricular dysfunction. Circ Res 2006;98:1177–85.

38. Rathmell JC, Thompson CB. The central effectors of cell death in the immune system. Annu Rev Immunol 1999;17:781–828.

39. Vermes I, Haanen C, Reutelingsperger C. Flow cytometry of apoptotic cell death. J Immunol Methods 2000;243:167–90.

40. Barreau C, Paillard L, Osborne HB. AU-rich elements and associated factors: are there unifying principles? Nucleic Acids Res 2005;33:7138–50.

41. Vasudevan S, Steitz JA. AU-rich-element-mediated upregulation of translation by FXR1 and Argonaute 2. Cell 2007;128:1105–18.

42. Eulalio A, Behm-Ansmant I, Izaurralde E. P bodies: at the crossroads of post-transcriptional pathways. Nat Rev Mol Cell Biol 2007;8:9–22.

43. Vinuesa CG, Cook MC, Angelucci C, et al. A RING-type ubiquitin ligase family member required to repress follicular helper T cells and autoimmunity. Nature 2005;435:452–8.

44. Yu D, Tan AH, Hu X, et al. Roquin represses autoimmunity by limiting inducible T-cell co-stimulator messenger RNA. Nature 2007;450:299–303.

45. Niu J, Azfer A, Zhelyabovska O, Fatma S, Kolattukudy PE. Monocyte chemotactic protein (MCP)-1 promotes angiogenesis via a novel transcription factor, MCP-1-induced protein (MCPIP). J Biol Chem 2008;283:14542–51.

46. Okamura A, Iwata N, Nagata A, et al. Involvement of casein kinase Iε in cytokine-induced granulocytic differentiation. Blood 2004;103:2997–3004.

47. Iwata N, Murayama T, Matsumori Y, et al. Autocrine loop through cholecystokinin-B/gastrin receptors involved in growth of human leukemia cells. Blood 1996;88:2683–9.

48. Rodriguez-Tarduchy G, Collins M, Lopez-Rivas A. Regulation of apoptosis in interleukin-3-dependent hemopoietic cells by interleukin-3 and calcium ionophores. EMBO J 1990;9:2997–3002.